A ~3.8 hr Periodicity From an Ultrasoft Active Galactic Nucleus Candidate

Dacheng Lin – University of Alabama

Jimmy A. Irwin – University of Alabama

Olivier Godet – Université de Toulouse

Natalie A. Webb – Université de Toulouse

Didier Barret – Université de Toulouse

Citation of published version:

Lin, D., Irwin, J., Godet, O., Webb, N., Barret, D. (2013): A ~3.8 hr Periodicity From an Ultrasoft Active Galactic Nucleus Candidate. *The Astrophysical Journal Letters*, 776(1). http://dx.doi.org/10.1088/2041-8205/776/1/L10

The Astrophysical Journal Letters, 776:L10 (6pp), 2013 October 10 doi:10.1088/2041-8205/776/1/L10

A ∼ 3.8 hr PERIODICITY FROM AN ULTRASOFT ACTIVE GALACTIC NUCLEUS CANDIDATE

Dacheng Lin[1], Jimmy A. Irwin[1], Olivier Godet[2,3], Natalie A. Webb[2,3], and Didier Barret[2,3]
[1] Department of Physics and Astronomy, University of Alabama, Box 870324, Tuscaloosa, AL 35487, USA; dlin@ua.edu
[2] CNRS, IRAP, 9 avenue du Colonel Roche, BP 44346, F-31028 Toulouse Cedex 4, France
[3] Université de Toulouse, UPS-OMP, IRAP, F-31400 Toulouse, France
Received 2013 July 28; accepted 2013 September 5; published 2013 September 25

ABSTRACT

Very few galactic nuclei are found to show significant X-ray quasi-periodic oscillations (QPOs). After carefully modeling the noise continuum, we find that the ∼3.8 hr QPO in the ultrasoft active galactic nucleus candidate 2XMM J123103.2+110648 was significantly detected (∼5σ) in two *XMM-Newton* observations in 2005, but not in the one in 2003. The QPO root mean square (rms) is very high and increases from ∼25% in 0.2–0.5 keV to ∼50% in 1–2 keV. The QPO probably corresponds to the low-frequency type in Galactic black hole X-ray binaries, considering its large rms and the probably low mass (∼10^5 $M_\odot$) of the black hole in the nucleus. We also fit the soft X-ray spectra from the three *XMM-Newton* observations and find that they can be described with either pure thermal disk emission or optically thick low-temperature Comptonization. We see no clear X-ray emission from the two *Swift* observations in 2013, indicating lower source fluxes than those in *XMM-Newton* observations.

Key words: accretion, accretion disks – black hole physics – X-rays: galaxies – X-rays: individual (2XMM J123103.2+110648)

Online-only material: color figures

1. INTRODUCTION

Although a large variety of X-ray quasi-periodic oscillations (QPOs) have been observed in Galactic black hole X-ray binaries (BHBs), they are hardly seen in galactic nuclei, which are believed to harbor supermassive black holes (SMBHs, black hole (BH) mass $M_{\rm BH} \gtrsim 10^5\ M_\odot$). If BH-mass scaling works, QPOs from SMBHs will have much longer timescales and thus be much better resolved in time than those from BHBs. Therefore QPOs from SMBHs can shed new lights on the origin of QPOs and in turn on the behavior of accretion flows onto BHs. Currently the two most confident cases are the ∼1.0 hr QPO from the active galactic nucleus (AGN) RE J10341+396 (∼5.6σ, Gierliński et al. 2008; but see Vaughan (2010)) and the ∼200 s one from Swift J164449.3+573451 (∼4.3σ; Reis et al. 2012), a tidal disruption event (TDE) candidate, in which a star approaching the central SMBH was tidally disrupted and subsequently accreted.

We discovered 2XMM J123103.2+110648 (J1231+1106 hereafter) as a very soft source, untypical of AGNs, in our project of classifications of 4330 X-ray sources from the 2XMMi-DR3 catalog (Lin et al. 2012). We have reported some results of our study of this source in Lin et al. (2013), including the discovery of a possibly strong but transient QPO and very soft spectra (characteristic blackbody (BB) temperatures of 0.1–0.15 keV, no significant emission above 2 keV) from three *XMM-Newton* observations. This source was also independently discovered by Terashima et al. (2012), who also reported its very soft spectra and possible presence of a QPO, which, however, did not seem statistically significant to them. They suggested the source as an AGN, considering its coincidence with a slightly extended Sloan Digital Sky Survey source. Ho et al. (2012) obtained a Magellan optical spectrum of this counterpart in 2012, which exhibited as a Type 2 AGN (redshift $z = 0.11871$, the source luminosity distance of 532 Mpc, assuming a flat universe with $H_0 = 73$ km s^{-1} Mpc^{-1} and $\Omega_{\rm M} = 0.27$). The narrow lines have very small velocity dispersions ($\sigma = 33.5$ km s^{-1} for [O III] λ5007), suggesting a small BH mass (∼10^5 $M_\odot$).

In this Letter we continue to study J1231+1106. Different from Lin et al. (2013), we calculate the significance of the QPO formally, carry out detailed spectral fits, concentrating on the physical model by Done et al. (2012), and present two *Swift* follow-up observations. In Section 2, we describe the data analysis. In Section 3, we present the results. The conclusions and the discussion of the source nature are given in Section 4.

2. DATA ANALYSIS

J1231+1106 was serendipitously detected at off-axis angles of ∼6′ in three *XMM-Newton* observations (XMM1, XMM2, and XMM3 hereafter; see Table 1) of the quasar LBQS 1228+1116. XMM1 was made in 2003 July, and XMM2 and XMM3 in 2005 December, with only 4 days apart. We used the X-ray light curves, energy and power spectra obtained in Lin et al. (2013), which we refer to for details. One exception is that here we combined data from all available cameras (i.e., pn, MOS1 and MOS2; the source was not in the field of view of MOS1 in XMM2 and XMM3) and used the MOS time resolution (2.6 s) as the light curve bin size to produce the power spectra.

The QPO in J1231+1106 has most power in one frequency bin in the unbinned power spectra and has some underlying red noise, except the Poisson noise. To quantify its significance, we used the maximum likelihood method (Vaughan 2005; Barret & Vaughan 2012), in which, one first obtains the probability distribution of the true power continuum through maximum likelihood fitting of the power spectra and then calculates the QPO significance assuming that the observed power, after being normalized by the true power and multiplied by a factor of two, follows a χ^2 distribution with two degrees of freedom. We fitted the spectra below 0.1 Hz, ignoring five frequency bins centering on the QPO centroid frequency in the fits, in order to exclude the possible QPO contamination. We focused on a single powerlaw (PL) model (depending on the frequency f in the form of $f^{-\Gamma_{\rm PL}}$) for the red noise. The best-fitting values of $\Gamma_{\rm PL}$ are ∼1.5 but not well constrained. In the final fits we assumed $\Gamma_{\rm PL}$ to be within 1–2, a range often seen in AGNs (e.g., Gierliński et al. 2008; McHardy 2010). To assess the limits of our modeling of the red

Table 1
Properties of J1231+1106 in Three *XMM-Newton* Observations

	0145800101 (XMM1)	0306630101 (XMM2)	0306630201 (XMM3)
Observation Date	2003 Jul 13	2005 Dec 13	2005 Dec 17
Exposure (ks, pn/MOS1/MOS2)	45.4/58.0/61.4	54.8/–/68.7	80.8/–/92.2
Power spectra			
Bin size (μHz)	18.2	14.6	10.4
QPO quality factor	...	>5	>7
Hard lag (ks)[a]	...	0.4 ± 0.6	1.1 ± 0.5
QPO rms (%, 0.2–2 keV)[b]	0 ± 9	30.8 ± 0.5	24.7 ± 0.3
QPO rms (%, 0.2–0.5 keV)[b]	0 ± 9	27.8 ± 0.4	24.2 ± 0.4
QPO rms (%, 0.5–1 keV)[b]	0 ± 10	32.1 ± 0.5	21.9 ± 0.6
QPO rms (%, 1–2 keV)[b]	0 ± 20	44 ± 2	56 ± 2
Energy spectral fits[c]			
Model (a): BB			
$N_{\rm H}$ (10^{20} cm^{-2})		<0.4	
$kT_{\rm BB}$ (keV)	0.125 ± 0.005	0.151 ± 0.004	0.134 ± 0.003
$N_{\rm BB}$	42 ± 10	37 ± 5	47 ± 6
$\chi^2_\nu(\nu)$	1.29(72)	1.16(142)	1.08(144)
Model (b): MCD			
$N_{\rm H}$ (10^{20} cm^{-2})		$0.6^{+1.8}$	
$kT_{\rm MCD}$ (keV)	0.16 ± 0.01	0.20 ± 0.01	0.18 ± 0.01
$N_{\rm MCD}$	12^{+7}_{-3}	9^{+4}_{-2}	13^{+6}_{-3}
$\chi^2_\nu(\nu)$	1.15(72)	1.04(142)	1.04(144)
$F_{\rm abs}$ (10^{-13} erg s^{-1} cm^{-2})[d]	0.48 ± 0.03	1.06 ± 0.04	0.77 ± 0.03
$F_{\rm unabs}$ (10^{-13} erg s^{-1} cm^{-2})[d]	$0.65^{+0.10}_{-0.06}$	$1.38^{+0.18}_{-0.09}$	$1.04^{+0.15}_{-0.08}$
Model (c): optxagnf (non-rotating, pure thermal disk)			
$N_{\rm H}$ (10^{20} cm^{-2})		$0.2^{+1.8}$	
$M_{\rm BH}$ ($M_\odot$)		$(4.2^{+0.9}_{-0.2}) \times 10^4$	
$L_{\rm Bol}/L_{\rm Edd}$	0.92 ± 0.05	1.77 ± 0.08	1.3 ± 0.05
$\chi^2_\nu(\nu)$	1.16(72)	1.09(142)	1.07(144)
Model (d): optxagnf (maximally rotating, pure thermal disk)			
$N_{\rm H}$ (10^{20} cm^{-2})		$0.2^{+1.8}$	
$M_{\rm BH}$ ($M_\odot$)		$(3.2^{+0.7}_{-0.2}) \times 10^5$	
$L_{\rm bol}/L_{\rm Edd}$	0.110 ± 0.006	0.213 ± 0.009	0.162 ± 0.007
$\chi^2_\nu(\nu)$	1.16(72)	1.09(142)	1.07(144)
Model (e): optxagnf (non-rotating, $r_{\rm cor} = 50r_{\rm g}$, $M_{\rm BH} = 10^5\ M_\odot$)			
$N_{\rm H}$ (10^{20} cm^{-2})		2^{+5}	
$L_{\rm bol}/L_{\rm Edd}$	$0.6^{+0.4}_{-0.2}$	$1.0^{+0.6}_{-0.3}$	$0.8^{+0.5}_{-0.2}$
$kT_{\rm e}$ (keV)	0.14 ± 0.01	0.18 ± 0.01	0.16 ± 0.01
τ		29 ± 10	
$\chi^2_\nu(\nu)$	1.17(71)	1.05(141)	1.05(143)
Model (f): optxagnf (non-rotating, $r_{\rm cor} = 50r_{\rm g}$, including Sw2/UVW2)			
$N_{\rm H}$ (10^{20} cm^{-2})		2^{+5}	
$M_{\rm BH}$ ($M_\odot$)		$(2.0^{+1.9}_{-1.1}) \times 10^6$	
$L_{\rm bol}/L_{\rm Edd}$	$0.07^{+0.15}_{-0.04}$	$0.10^{+0.19}_{-0.07}$	$0.09^{+0.20}_{-0.05}$
$kT_{\rm e}$ (keV)	0.15 ± 0.01	0.18 ± 0.01	0.16 ± 0.01
τ		25 ± 8	
$\chi^2_\nu(\nu)$	1.19(70)	1.05(140)	1.06(142)
***XMM-Newton* OM photometry**			
V flux[e] and AB Mag	2.2 ± 1.3, 20.5 ± 0.6	3.8 ± 1.1, 20.0 ± 0.3	3.0 ± 1.1, 20.2 ± 0.4
B flux[e] and AB Mag	... ...	2.2 ± 0.6, 21.0 ± 0.3	2.0 ± 0.7, 21.1 ± 0.4
U flux[e] and AB Mag	1.4 ± 0.7, 22.0 ± 0.6	1.2 ± 0.6, 22.2 ± 0.6	2.0 ± 0.6, 21.6 ± 0.3
UVW1 flux[e] and AB Mag	1.6 ± 1.0, 22.2 ± 0.7	... ...	2.1 ± 0.9, 22.0 ± 0.5

Notes.
[a] The time lag of hard X-rays (1–2 keV) behind soft X-rays (0.2–0.5 keV), with 1σ errors from the red and Poisson noises.
[b] The QPO fractional rms (Poisson and red noises subtracted) using the power at the bin containing the QPO centroid frequency, with 1σ errors from the red and Poisson noises.
[c] All errors are at a 90% confidence level.
[d] The 0.3–10 keV absorbed ($F_{\rm abs}$) and unabsorbed ($F_{\rm unabs}$) fluxes.
[e] In units of 10^{-17} erg s^{-1} cm^{-2} Å^{-1}.

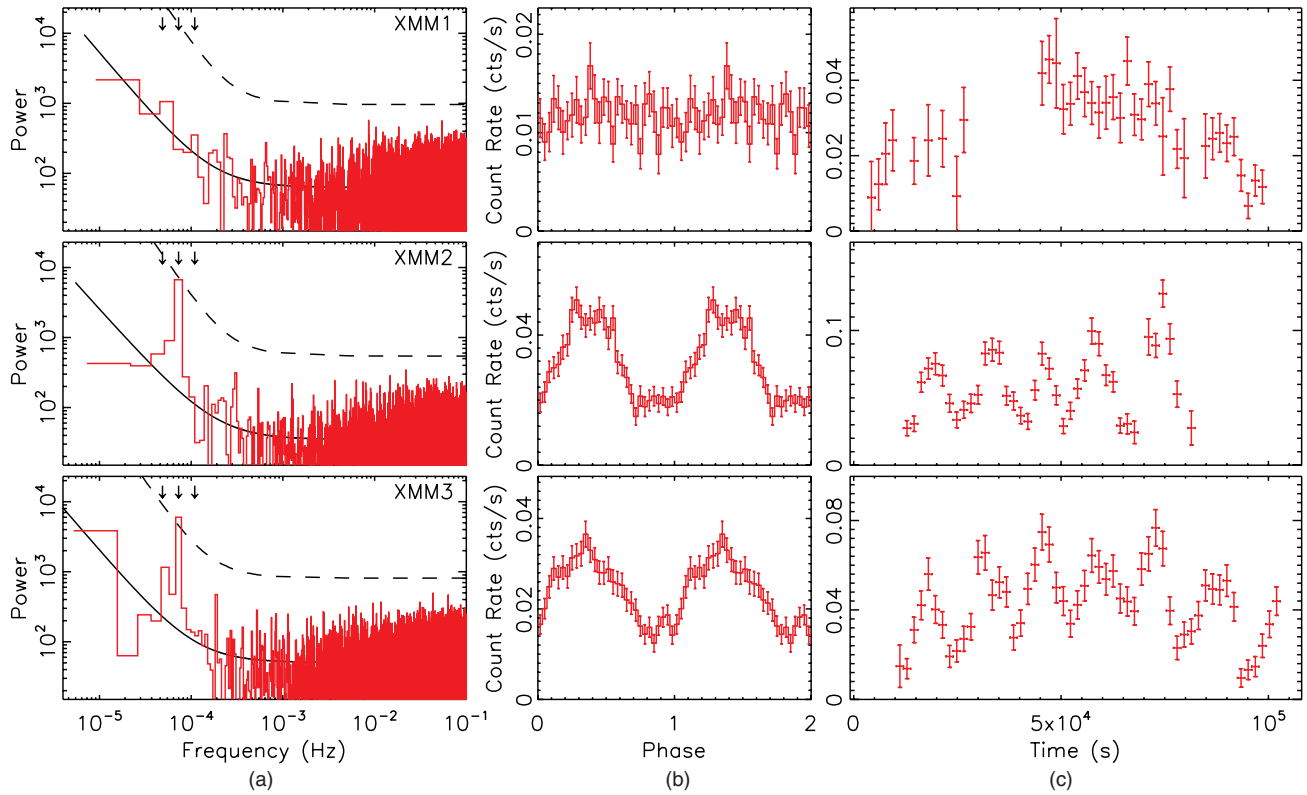

Figure 1. (a) The power spectra normalized to $(\mathrm{rms/mean})^2/\mathrm{Hz}$. The arrows mark the periods of $3P_0/2$, P_0, $2P_0/3$ ($P_0 = 13{,}710$ s, see Figure 2(a)). The solid lines are the best-fitting PL model to the red noise plus Poisson noise. The dashed lines are the 99.9% confidence detection level. The power spectrum of XMM1 is from the second segment of data (after 40 ks in the light curve plot in the top right panel) because of frequent strong background flares in earlier data. (b) The light curves folded at P_0. (c) The unfolded light curves, shifted in time to be in phase. All panels use 0.2–2 keV events from all available cameras, except (c), which uses only the pn data.

(A color version of this figure is available in the online journal.)

noise, we also tested a PL model with $0 < \Gamma_{\rm PL} < 3$ and a broken PL model with the indices below ($\Gamma_{1,\rm PL}$) and above ($\Gamma_{2,\rm PL}$) the break frequency assuming typical values (($\Gamma_{1,\rm PL}$, $\Gamma_{2,\rm PL}$) = (1, 2), (1, 3), and (0, 2)) seen in the literature (Gierliński et al. 2008; McHardy 2010; Reis et al. 2012). The break frequency was allowed to be free. The Poisson noise was modeled with a constant fixed at the value inferred from power above 0.1 Hz (it deviated from the expected value by <0.3%). To further account for the effect of data incompleteness due to background flares, we carried out Monte Carlo simulations following Timmer & Koenig (1995). For each model each observation, 10^7 light curves following the power spectral distribution inferred above from the maximum likelihood method and having the same mean count rate, variance, and sampling pattern as the observed light curves were generated and then used to produce the power spectra and obtain the QPO significance based on the distribution of simulated power at the QPO frequency.

We fitted the X-ray spectra with several models: a single-temperature BB, a multicolor disk (MCD), and the AGN spectral model optxagnf by Done et al. (2012). They are *bbodyrad*, *diskbb*, and *optxagnf*, respectively, in XSPEC. Both the BB and MCD models were redshifted by $z = 0.11871$ using the *zashift* model in XSPEC (the optxagnf model has handled this internally). All models included the Galactic absorption fixed at $N_{\rm H} = 2.3 \times 10^{20}$ cm^{-2} (Kalberla et al. 2005) using the *wabs* model. Possible absorption intrinsic to the source was accounted for using the *zwabs* model, with the column densities tied to be the same in all observations because they were consistent within the 90% errors.

We also obtained the magnitudes and fluxes in the Optical Monitor (OM; Mason et al. 2001) filters, with the *omichain* task in the SAS 11.0.0 package (Table 1). We note that the B and UVW1 filters were not used in XMM1 and XMM2, respectively, and that the source was not detected in the UVM2 or UVW2 filters in any observation.

At our request, *Swift* (Gehrels et al. 2004) observed J1231+1106 twice, once on 2013 March 8 (observation ID: 00032732001, Sw1 hereafter) and the other on 2013 June 21 (observation ID: 00032732001, Sw2 hereafter). The X-Ray Telescope (XRT; Burrows et al. 2005) was operated in photon counting mode for 8.5 ks and 4.4 ks, respectively. The UV–Optical Telescope (Roming et al. 2005) used the UVW1 filter (8.3 ks) in Sw1 and the UVW2 filter (4.3 ks) in Sw2. We analyzed the data with FTOOLS 6.13 and the calibration files of 2013 July. The source was hardly detected in the XRT. We calculated the count rate confidence intervals using Bayesian statistics (Kraft et al. 1991), with radii of 20″ and 2′ for the circular source and background regions, respectively. The UV magnitudes and fluxes were measured with the task *uvotsource* with radii of 5″ and 25″ for the circular source and background regions, respectively.

3. RESULTS

3.1. The ∼3.8 hr QPO

Figures 1 and 2 show the timing properties of J1231+1106 (see also Figure 6 in Lin et al. 2013). As obtained by Lin et al. (2013), the source showed a large coherent oscillation at a period

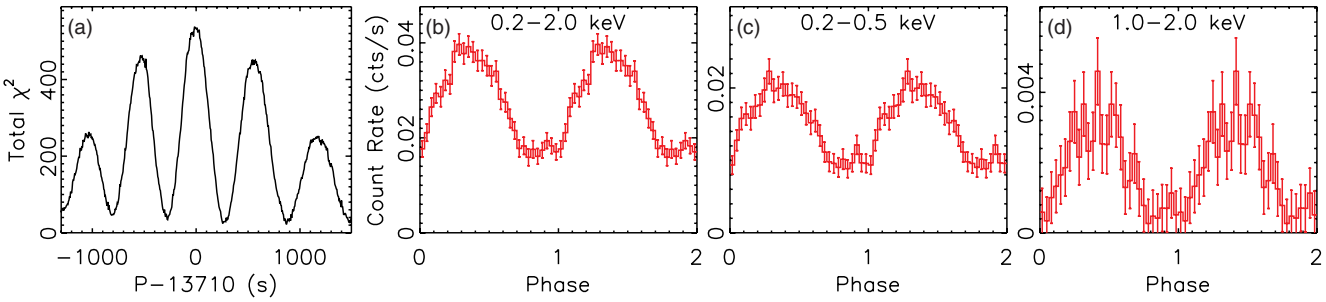

Figure 2. (a) The total χ^2 values from the fits with a constant to the 0.2–2 keV light curves folded at various tentative periods. (b)–(d) The 0.2–2 keV, 0.2–0.5 keV and 1–2 keV light curves folded at $P_0 = 13710$ s, respectively. All panels use XMM2 and XMM3 data only.

(A color version of this figure is available in the online journal.)

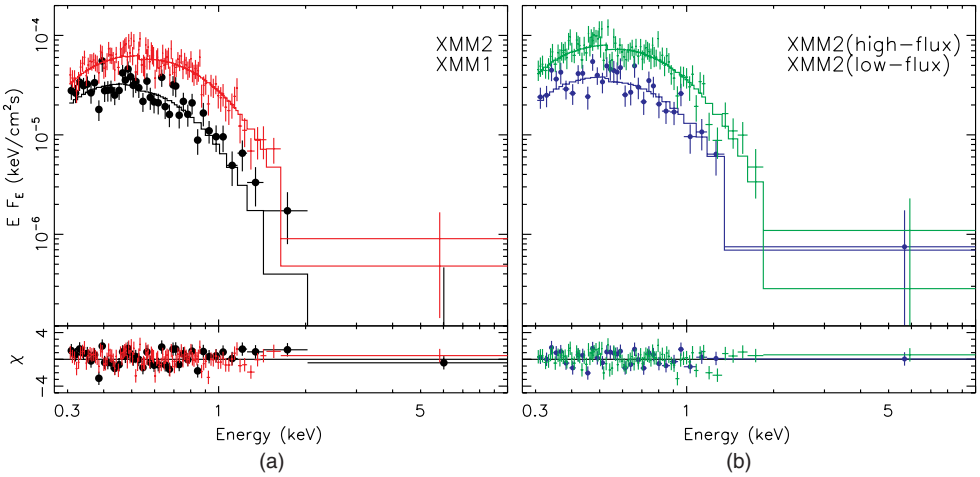

Figure 3. Unfolded spectra and the fit residuals of J1231+1106 using the MCD model. (a) XMM1 (black filled circles) and XMM2 (red); (b) the spectrum in the high-flux interval (green) and that in the low-flux interval (blue filled circled) in XMM2. For clarity, we show the pn camera only and have the data rebinned.

(A color version of this figure is available in the online journal.)

about 3.8 hr in the two observations (XMM2 and XMM3) in 2005 December but not clearly in the one (XMM1) in 2003 July. The QPO concentrates in one frequency bin (Figure 1(a)), and the quality factor, defined as the centroid frequency divided by the frequency width (full-width at half-maximum), is >7 (Table 1). The oscillation is only quasi-periodic, considering that the minima and maxima of the light curves in XMM2 and XMM3 do not seem to be well in phase (Figure 1(c)).

Assuming blind search over frequencies below 0.1 Hz (the highest stable orbital frequency around a non-rotating BH of $2 \times 10^4\ M_\odot$) in each observation separately, we obtained the 99.9% confidence limit in Figure 1(a) (the dashed line) and the QPO significance at the 3.1σ (Gaussian probability, the same below) and 4.0σ levels in XMM2 and XMM3, respectively, assuming the PL model for the red noise ($1 < \Gamma_{\rm PL} < 2$, 0.2–2 keV). Considering that the QPO was detected at the same frequency in two observations, its global significance is 6.7σ. The Monte Carlo simulations confirmed the significance to be $>6.2\sigma$. The significance is 5.1σ if we assumed $0 < \Gamma_{\rm PL} < 3$. Using the broken PL model for the red noise, the QPO significance is 6.4σ, 5.4σ and 5.9σ for $(\Gamma_{1,\rm PL}, \Gamma_{2,\rm PL}) = (1, 2)$, (1, 3) and (0, 2), respectively, from Monte Carlo simulations. The fractional root-mean-square (rms) variability in the QPO is remarkably high and increases from ∼25% in 0.2–0.5 keV to ∼50% in 1–2 keV in both XMM2 and XMM3 but is consistent with zero in XMM1 (Table 1). The folded light curves in these two energy bands are plotted in Figure 2, and we see no clear time lag between them ($\lesssim$1.1 ks from Table 1).

3.2. The Ultrasoft X-Ray Spectra

The fitting results of the *XMM-Newton* observations with various models are given in Table 1. We concentrated on X-ray spectra, because in optical the source appeared red (Table 1) and should be dominated by galaxy emission, instead of nuclear accretion, as often seen in low-mass AGNs (Done et al. 2012). In the UV, the source was detected in the UVW1 filter, but with large uncertainties. It still appeared a little red in the UVW1 and UVW2 filters from the two *Swift* observations (Section 3.3). Thus we will refer to the shortest-wavelength detection, i.e., the UVW2 one in Sw2, as possible emission from nuclear accretion.

All three spectra are very soft, with $kT_{\rm BB} \sim 0.13$–0.15 keV or $kT_{\rm MCD} \sim 0.16$–0.20 keV (source rest frame). The fits with the BB model show systematic residuals, which are unseen using the MCD model (Figure 3(a)). Both models infer little intrinsic absorption. We see that the inner disk temperature varies at a significance level of 4.8σ while the inner disk radius is consistent within the 90% confidence errors in these observations, implying the disk luminosity L to approximately follow the relation of $L \propto T_{\rm MCD}^4$. The source reached a peak 0.3–10 keV absorbed luminosity of 3.6×10^{42} erg s^{-1} and a bolometric unabsorbed luminosity of 8.5×10^{42} erg s^{-1} (the MCD model) in XMM2. XMM1 is the faintest, with a 0.3–10 keV absorbed luminosity of 1.6×10^{42} erg s^{-1} and a bolometric unabsorbed luminosity of 5.0×10^{42} erg s^{-1}. Both the BB and MCD models under-predicted the Sw2/UVW2 flux, by a factor of $\sim 2 \times 10^4$ and 48, respectively (using

the best-fitting model to XMM1 and assuming the reddening $E(B-V) = 1.7 \times 10^{-22} N_{\rm H}$, the same below).

We used the MCD model to check the spectral variability in the oscillation. We created and fitted two spectra from XMM2 from the high-flux and low-flux intervals, corresponding to the pn 1 ks 0.2–2 keV count rate higher and lower than 0.05 counts s^{-1}, respectively. The column density was fixed at the value obtained above from the simultaneous fit to all three *XMM-Newton* observations. The best-fitting models are shown in Figure 3(b). We inferred a lower temperature and a smaller inner radius of the disk in the low-flux interval than in the high-flux interval, but only at a 1.7σ confidence level.

We next look at the optxagnf model. It assumes that the gravitational energy released in the disk is emitted as a color-corrected BB down to a (coronal) radius $r_{\rm cor}$, while within this radius the available energy is distributed between powering two Comptonization components: the soft one via Comptonization in an optically thick cool corona and the hard one in an optically thin hot corona.

Considering the very soft spectra, we first investigated the scenario of pure thermal disk emission (setting $r_{\rm cor}$ to be at the innermost stable circular orbit (ISCO)). The fitting results for two cases are given in Table 1: a non-rotating Schwarzschild BH (Models (c)) and a maximally rotating Kerr BH (Models (d)). They inferred $M_{\rm BH} = 4 \times 10^4\ M_\odot$ and $3 \times 10^5\ M_\odot$, and the Eddington ratio $L_{\rm Bol}/L_{\rm Edd} \sim$ 1–2 and ~0.1–0.2, respectively. Both cases under-predicted the Sw2/UVW2 flux by a factor of ~20.

We then considered soft Comptonization to describe the spectra (no hard Comptonization because of no clear hard X-ray emission). We found that the data could not constrain all parameters well. We thus only report two special cases in Table 1: the first case assumes $M_{\rm BH} = 10^5\ M_\odot$ (Model (e)), and the second case includes the Sw2/UVW2 detection in the fits (Model (f)). Because the optical depth τ of the corona was found to be consistent within the 90% errors, we tied it to be the same for all observations in both cases. We found that the former case under-predicted the Sw2/UVW2 flux by a factor of 11. In the latter case, $M_{\rm BH} \sim 2 \times 10^6\ M_\odot$ and $L_{\rm Bol}/L_{\rm Edd} \sim$ 0.09–0.14 were inferred.

3.3. The Swift Follow-up Observations

The source was not detected in the XRT in either *Swift* observation. We estimated a 0.3–2 keV count rate of $(2^{+4}) \times 10^{-4}$ counts s^{-1} and $(5^{+8}) \times 10^{-4}$ counts s^{-1} (the errors are the 90% confidence bounds) from Sw1 and Sw2, corresponding to a 0.3–10 keV absorbed luminosity of $(3^{+5}) \times 10^{41}$ erg s^{-1} and $(7^{+11}) \times 10^{41}$ erg s^{-1} (based on the MCD fit to XMM1), respectively. Thus the source probably has become fainter. In the UV, we obtained the Sw1/UVW1 flux of $(1.4 \pm 0.2) \times 10^{-17}$ erg s^{-1} cm^{-2} $Å^{-1}$ (AB Mag of 22.7 ± 0.2), and the Sw2/UVW2 flux of $(1.1 \pm 0.3) \times 10^{-17}$ erg s^{-1} cm^{-2} $Å^{-1}$ (AB Mag of 23.4 ± 0.3).

4. DISCUSSION AND CONCLUSIONS

We have shown that J1231+1106 exhibited a ~3.8 hr QPO in the two *XMM-Newton* observations in 2005 at a $\sim 5\sigma$ significance level, making it one of the very few SMBHs with an X-ray QPO significantly detected. Its rms generally increases with energy, a trend also observed in most QPOs in Galactic BHBs and that in RE J10341+396 (Remillard & McClintock 2006; Middleton et al. 2009). Galactic BHBs can show both low-frequency (~0.1–30 Hz) and high-frequency (40–450 Hz) QPOs (Remillard & McClintock 2006). The former can have rms >15%, while the latter have rms ~1%. If the QPO in J1231+1106 corresponds to the low-frequency type in BHBs, we infer $M_{\rm BH} < 4 \times 10^6\ M_\odot$. High-frequency QPOs in BHBs sometimes display in pair with frequencies scaling in a 3:2 ratio and possibly following the relation of $f_0 = 931 (M_{\rm BH}/M_\odot)^{-1}$ Hz, where f_0 is the fundamental frequency of the pair (Remillard & McClintock 2006). Using this relation, $M_{\rm BH}$ in J1231+1106 is 2.6×10^7 or $3.8 \times 10^7\ M_\odot$, depending on whether we observed the periodicity of $2 f_0$ or $3 f_0$, respectively. If we assume instead the QPO centroid frequency to be the Keplerian frequency at the ISCO, $M_{\rm BH}$ would be within 3×10^7–$2 \times 10^8\ M_\odot$, depending on the spin of the BH. Considering the small BH mass ($\sim 10^5\ M_\odot$) inferred by Ho et al. (2012) from narrow optical emission lines and the large rms, the QPO in J1231+1106 is probably a low-frequency type. This QPO should have a different origin from those in RE J10341+396 and Swift J164449.3+573451 because the latter two QPOs are contributed mostly by the hard X-ray component (Middleton et al. 2011; Reis et al. 2012). Considering the probably high Eddington ratios of J1231+1106, the QPO could be due to thermal instability, which was often used to explain the "limit-cycle" behavior of the BHB GRS 1915+105 at high accretion rates (e.g., Zheng et al. 2011).

The ultrasoft X-ray spectra of J1231+1106 in the *XMM-Newton* observations appear broader than a single-temperature BB, but can be described well with either pure thermal disk emission or soft Comptonization, with $M_{\rm BH}$ consistent with that inferred from narrow optical emission lines. The former model is supported by the observation of the disk luminosity approximately following the relation of $L \propto T_{\rm MCD}^4$ expected for a standard disk, although the dynamical range is small (only a factor of ~2). The latter model is supported by the detection of the QPO, which, in the case of Galactic BHBs, often occurs in states with strong Comptonization (Remillard & McClintock 2006). Both models under-predict the Sw2/UVW2 flux by more than one order of magnitude, unless, for the soft Comptonization model, we assumed a BH mass ($\sim 10^6\ M_\odot$) much larger than that inferred from narrow optical emission lines and Eddington ratios (~0.1) too low to see strong soft Comptonization (Terashima et al. 2012). Thus the Sw2/UVW2 flux is probably dominated by galaxy emission.

Therefore, both the strong fast variability, whose power is mostly in the QPO, and the spectral modeling suggest J1231+1106 as a relatively small BH accreting at high rates. This is a popular explanation for narrow line Seyfert 1 galaxies (e.g., Boller et al. 1996; Grupe et al. 2010), and J1231+1106 could be an extreme case of such object, with only soft excess (see also Terashima et al. 2012). Alternatively, the source could be in a pure thermal state hardly observed in AGNs. This scenario was suggested by Miniutti et al. (2013) for GSN 069, a source showing many similarities as J1231+1106 (e.g., no hard X-ray detection, strong fast variability, and no broad H_α or H_β lines) and having UV-to-X-ray spectra consistent with pure thermal disk emission. In either case, the non-detection of broad H_α or H_β lines in J1231+1106 should indicate their absence, instead of being hiddened. This could be because the source had too weak hard X-ray emission to maintain the broad line region in equilibrium, or because the source only entered the current bright state recently, leaving no enough time to form the mature broad line region (Miniutti et al. 2013).

However, ultrasoft X-ray spectra are more commonly seen in TDEs. Such events are expected to rise on timescales of

months and decay on timescales of years, with the accretion rate approximately following $t^{-5/3}$, where t is the time since disruption, if the disrupted stars are solar-type (Rees 1988, 1990). About a dozen TDE candidates have been found (e.g., Komossa 2002; Lin et al. 2011). For J1231+1106, XMM1 is ∼2.5 yr before XMM2 and XMM3, with comparable fluxes. If it is a TDE, XMM1 should be in the rising phase, and XMM2 and XMM3 in the decay. The bolometric luminosity in 2013 would then decrease from those in XMM2 and XMM3 by a factor of ∼10, consistent with the *Swift* observations. The absence of broad H_α or H_β lines in the Magellan spectrum in 2012 could be because the source is too faint now, and the narrow emission lines are light echo from the TDE. Alternatively, the disrupted star is an evolved one, in which case the events have much longer timescales than those involving solar-type stars (MacLeod et al. 2012; this might also explain GSN 069, which showed no significant variability in the ∼1 yr monitoring by *Swift* in 2010–2011, but at fluxes a factor of >240 of those in the *ROSAT* observations in 1994). Under the TDE explanation, the QPO could be due to the special accretion mode in such events.

We want to thank the *Swift* PI Neil Gehrels for approving our ToO request to observe J1231+1106 twice. This work is supported by NASA Grant NNX10AE15G.

REFERENCES

Barret, D., & Vaughan, S. 2012, ApJ, 746, 131
Boller, T., Brandt, W. N., & Fink, H. 1996, A&A, 305, 53
Burrows, D. N., Hill, J. E., Nousek, J. A., et al. 2005, SSRv, 120, 165
Done, C., Davis, S. W., Jin, C., Blaes, O., & Ward, M. 2012, MNRAS, 420, 1848
Gehrels, N., Chincarini, G., Giommi, P., et al. 2004, ApJ, 611, 1005
Gierliński, M., Middleton, M., Ward, M., & Done, C. 2008, Natur, 455, 369
Grupe, D., Komossa, S., Leighly, K. M., & Page, K. L. 2010, ApJS, 187, 64
Ho, L. C., Kim, M., & Terashima, Y. 2012, ApJL, 759, L16
Kalberla, P. M. W., Burton, W. B., Hartmann, D., et al. 2005, A&A, 440, 775
Komossa, S. 2002, in Reviews in Modern Astronomy, Vol. 15, ed. R. E. Schielicke (New York: Wiley), 27
Kraft, R. P., Burrows, D. N., & Nousek, J. A. 1991, ApJ, 374, 344
Lin, D., Carrasco, E. R., Grupe, D., et al. 2011, ApJ, 738, 52
Lin, D., Webb, N. A., & Barret, D. 2012, ApJ, 756, 27
Lin, D., Webb, N. A., & Barret, D. 2013, arXiv:1309.0509
MacLeod, M., Guillochon, J., & Ramirez-Ruiz, E. 2012, ApJ, 757, 134
Mason, K. O., Breeveld, A., Much, R., et al. 2001, A&A, 365, L36
McHardy, I. 2010, in The Jet Paradigm, ed. T. Belloni (Lecture Notes in Physics, Vol. 794; Berlin: Springer), 203
Middleton, M., Done, C., Ward, M., Gierliński, M., & Schurch, N. 2009, MNRAS, 394, 250
Middleton, M., Uttley, P., & Done, C. 2011, MNRAS, 417, 250
Miniutti, G., Saxton, R. D., Rodríguez-Pascual, P. M., et al. 2013, MNRAS, 433, 1764
Rees, M. J. 1988, Natur, 333, 523
Rees, M. J. 1990, Sci, 247, 817
Reis, R. C., Miller, J. M., Reynolds, M. T., et al. 2012, Sci, 337, 949
Remillard, R. A., & McClintock, J. E. 2006, ARA&A, 44, 49
Roming, P. W. A., Kennedy, T. E., Mason, K. O., et al. 2005, SSRv, 120, 95
Terashima, Y., Kamizasa, N., Awaki, H., Kubota, A., & Ueda, Y. 2012, ApJ, 752, 154
Timmer, J., & Koenig, M. 1995, A&A, 300, 707
Vaughan, S. 2005, A&A, 431, 391
Vaughan, S. 2010, MNRAS, 402, 307
Zheng, S.-M., Yuan, F., Gu, W.-M., & Lu, J.-F. 2011, ApJ, 732, 52